Mechano-Chemical Stability of Gold Nanoparticles Coated with Alkanethiolate SAMs

Brian J. Henz[1], Takumi Hawa[2,3], and Michael R. Zachariah[2,3]

[1]U.S. Army Research Laboratory
Aberdeen Proving Ground, MD

[2]Departments of Mechanical Engineering and of Chemistry and Biochemistry
University of Maryland
College Park, MD

[3]National Institute of Standards and Technology
Gaithersburg, MD

Abstract
Molecular dynamics simulations are used to analyze the structure and stability of alkanethiolate self-assembled monolayers (SAMs) on gold nanoparticles. We have observed that the surface of gold nanoparticles become highly corrugated by the adsorption of the SAMs. Furthermore, as the temperature is increased, the SAMs dissolve into the gold nanoparticle, creating a liquid mixture at temperatures much lower than the melting temperature of the gold nanoparticle. By analyzing the mechanical and chemical properties of gold nanoparticles at temperatures below the melting point of gold, with different SAM chain lengths and surface coverage properties, we have determined that the system is metastable. The model and computational results that provide support for this hypothesis are presented.

1. Introduction and Background

Nanoparticles are often used in applications where a high surface area to volume ratio is desired. Some of the typical applications include catalysis, biosensors, and use as drug delivery vehicles.[1,2] A major limitation of the expanded use of these nanoparticles is that the fabrication of nanoparticles with the desired morphology and structure is challenging.[3,4,5] Gold is a commonly used material because of its resistance to oxidation and its interesting electrical, magnetic, optical, and physical properties[6]. Furthermore there is a considerable knowledge base on functionalizing gold surfaces that are being ported to analogous particles.[7] For this reason gold nanoparticles are commonly chosen for basic research because of the availability of experimental[8,9] and atomistic simulation data.[10,11] Using molecular dynamics (MD) simulations Lewis et al.[12] were able to determine the melting process for gold nanoparticles. This last result is important because the authors found that the surface atoms melt first, and at a temperature below that of the atoms in the core of the nanoparticle. The implications of this for coated nanoparticles is that the surface atoms, where binding of the monolayer takes place, is affected by a lower temperature than is expected from the melting temperature of the whole nanoparticle. The results of these past efforts are built upon in this work in order to analyze, and in larger gold nanoparticle and in particular the nature and role of surface functionalization.

Coating of gold surfaces and nanoparticles with a self-assembled monolayer (SAM) creates many additional applications including lithography, lubrication, catalysis, biocompatible materials, and biosensors.[6,13] There have been numerous experimental[14,15,16] and numerical[13,17,18] studies performed that have attempted to characterize the properties of alkanethiolate SAM coated gold surfaces. Simulations investigating alkanethiolate SAM coated gold surfaces accurately predict the c(4x2) superlattice structure of alkanethiols on an Au(111) surface. Additional work has predicted the segregation of SAM chains adsorbed on a gold surface by length, surface frictional forces[19], and phase behavior.[20] Efforts to characterize the alkanethiolate SAM coated gold nanoparticle system have been limited to atomistic simulations considering a single alkanethiol chain, and a small (less than 100 atom) gold cluster[17,21] or MD simulations of small nanoparticles that ignore gold-gold interactions.[6,18]

During the fabrication of nanoparticles the propensity to agglomerate and sinter must be inhibited by the passivation of the nanoparticle surface. The use of coatings for surface passivation has been found to significantly reduce the degree to which agglomeration and sintering will occur.[22] For instance, Hawa and Zachariah found that a hydrogen surface passivation coating used with a silicon nanoparticle will prevent reaction with other particles when collided at thermal velocities or will retard the process.[23] Other affects related to the passivation layer investigated computationally, include changes in the internal pressure and surface tension.[24]

2. Computational Modeling and Numerical Procedure

There are numerous documented MD studies of alkanethiolate SAMs on gold surfaces.[13,17,19] However, these studies have been limited to flat gold surfaces, or to fixed gold atoms in a nanocrystallite.[18,6] In addition to, and in support of, these previous MD simulations, *ab-initio* quantum chemical calculations have been used to simulate gold clusters with short alkanethiolate SAMs, primarily to determine potential parameters for MD or MC computations. The *ab-initio* calculations show that the gold crystal lattice is perturbed by the adsorbed ligand.[25] The consequence of the perturbation is an increase in Au-Au bond length of up to 20%. The increase in bond length is observed around the adsorption site with relaxation propagating to the second layer. These results suggest that the MD simulations should include dynamic gold atoms in order to accurately consider the nanoparticle/SAM system.

Alkanethiol chains adsorbed on a flat surface made of immobile gold atoms are limited to diffusion in only two dimensions, whereas, chains adsorbed onto a nanoparticle surface with mobile gold atoms may diffuse in three dimensions. This disparity in model detail is expected to provide more insight into the SAM coated nanoparticle system, than previously available. The inclusion in the simulation of a surface constructed of dynamic gold atoms should be able to more accurately predict alkanethiol chain movement than the limited movement possible on a flat surface of fixed gold atoms.

The size of the model system investigated here is determined by approximating experimentally realistic systems. The manufacture of consistently sized small diameter nanoparticles becomes more difficult at diameters of less than 50Å, therefore, in this work 50Å diameter gold nanoparticles (4093 gold atoms) with and without SAMs are considered. The SAM considered consists of alkanethiolate chains that contain a sulfur atom head group that binds to the gold surface, and a carbon backbone with 3 to 18 carbon atoms comprising the alkyl chain.

The MD simulations in this work are carried out using the LAMMPS (Large-scale Atomic/Molecular Massively Parallel Simulator)[26] software.

2.1. Simulating the Gold Substrate

In this effort the gold substrate atoms are explicitly considered as dynamic atoms, requiring that an accurate potential be used to simulate these atomic interactions. The embedded atom method[11,27,28] (EAM) has received much attention for accurately simulating atomic gold interactions and the interactions of other fcc lattice metals. This method uses empirical embedding functions that originate from density functional theory (DFT) and have been successfully used to model many of the physical properties of gold. We chose the EAM for modeling the gold substrate because of its reported accuracy, and the potentially important extensions developed for the EAM for modeling surfaces, such as the extended EAM[29] (XEAM), and the surface EAM (SEAM).[30] The actual EAM potential used in this work is taken from LAMMPS.

2.2. Modeling the Alkanethiolate Chain

The alkanethiolate polymer chain may be simulated with a range of computational complexity depending upon the resources available, and the accuracy of results required. For MD simulations, the three methods available for modeling the alkanethiol chain are the high-accuracy/high computational requirement all-atom model, the less accurate/lower computational requirement united atom method, and the coarse grained bond model. These methods can be compared by considering the CH_2 molecule that makes up the backbone of the alkanethiolate chain. When using the all-atom model, the numerical simulation must consider three particles for each molecule and the interactions between each. Using the united atom model only one particle is simulated for each molecule[31], which eliminates the intermolecular interactions, and limits the number of intermolecular interaction potentials required. Finally, with the coarse grained model, multiple molecules are clustered together into one particle with perhaps five or more CH_2 molecules grouped into one simulated particle.[32,33,34] For the simulations in this work we have chosen the united atom method, which is computationally more efficient than the all atom method, yet provides sufficient accuracy for the current analysis.

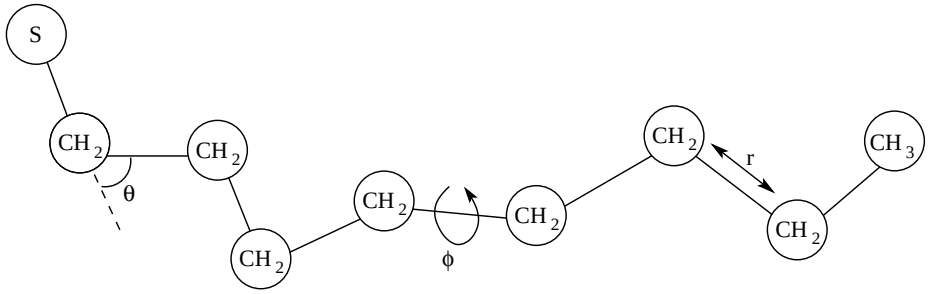

Figure 1. Sample alkanethiolate chain with 8 carbon atoms along the backbone.

The potentials and parameter values for the bending angle and dihedral angle from Figure 1 and used in this work are given in Shevade et al., the bond stretch parameters are given in Rai et al.[35]

2.3. Binding of Sulfur to Gold

The binding potential of the head sulfur atom of an alkanethiol chain to the gold substrate is of great interest as it affects the location, orientation, movement, and desorption of chains from the gold surface.[6,36,37] There has been much effort devoted to finding accurate potentials for simulating the sulfur to gold binding energy from ab-initio methods.[6,36] The most commonly published potentials resulting from these calculations are the 12-3 potential,[38] used most commonly in Monte Carlo (MC) simulations of alkanethiolates on gold[13,19] and the Morse potential, used in many of the MD simulation studies.[19,17,36,39] In addition to the issue of which potential best describes the binding between SAM headgroup and substrate, the possibility of SAM mobility must also be considered. Since the Morse potential, Eq. 1, can mimic a partially covalent bond, it is used in MD simulations along with the parameters given by Zhang et al to model the Au-S bond. The parameters for Eq. 1 are $D_e = 13.3$ kJ/mol, $\alpha = 1.38$, and $r_0 = 2.903$ Å.

$$U_{Morse}(r) = D_e\left[e^{-2\alpha(r-r_0)} - 2e^{-\alpha(r-r_0)}\right] \quad (1)$$

The binding energy of the alkanethiol to the gold surface has been determined to be around 184.1 kJ/mol when all of the sulfur-gold interactions are considered. Although this reported value is often referenced, their are several studies that report the sulfur-gold bond energy to be closer to 126.0 kJ/mol.[40,41] This discrepancy in the binding energy is large, and so in this work we will investigate using both binding energies in order to understand the affect that binding energy has on the computed results. For the sulfur-gold binding energy of 126.0 kJ/mol, the Morse potential parameter $D_e = 9.108$ kJ/mol.

3. Simulation Results

In this section, the results from the MD simulations are presented and analyzed. In order to study the affects of the alkanethiolate SAM on the gold nanoparticle we have computed many system properties. These properties include diffusion coefficients, radial pressure and density distributions, melting temperature, and the pair correlation function. A corrugation factor that describes the depth to which the gold surface is modified by the adsorbed alkanethiol chains is also defined in this section. Each of these results is a data point of the changes the nanoparticle surface experiences with the adsorption of the alkanethiolate SAM. For instance, the diffusion coefficient is used to compute the mobility of the SAM chains that are adsorbed on the surface of the nanoparticle, and the mobility of the gold atoms near the surface of the nanoparticle. The combination of these two coefficients will partially define the phase of the materials at and on the nanoparticle surface and also help in predicting if nucleation of the SAM chains will occur. Nucleation may occur under low surface coverage conditions when the chains form dense groups and uneven surface coverage. The density distribution is used to find the depth to which the sulfur atoms penetrate the surface of the gold nanoparticle and to compute the corrugation factor.

The simulation results will also be compared for the two sulfur-gold binding energies considered in this work. The computed results will be compared and discussed in order to better understand how the head group binding energy affects the properties of the nanoparticle and anticipated trends for these properties. It is expected that the lower binding energy will have less of an affect on the properties of the gold nanoparticle than the high binding energy. On the other hand some processes such as desorbtion will possibly be observed only at the lower binding energy because the temperature required for desorbtion will be lower. A detailed discussion of the model initialization can be found in Henz et al.[42]

3.1. Pair Correlation Function

The pair correlation function, $g(r)$, is defined as the number of atoms a distance r from a given atom compared with the number of atoms at the same distance in an ideal gas at the same density.[43] The pair correlation function for a bare 50Å diameter gold nanoparticle is shown in Figure 2 for a range of temperatures.

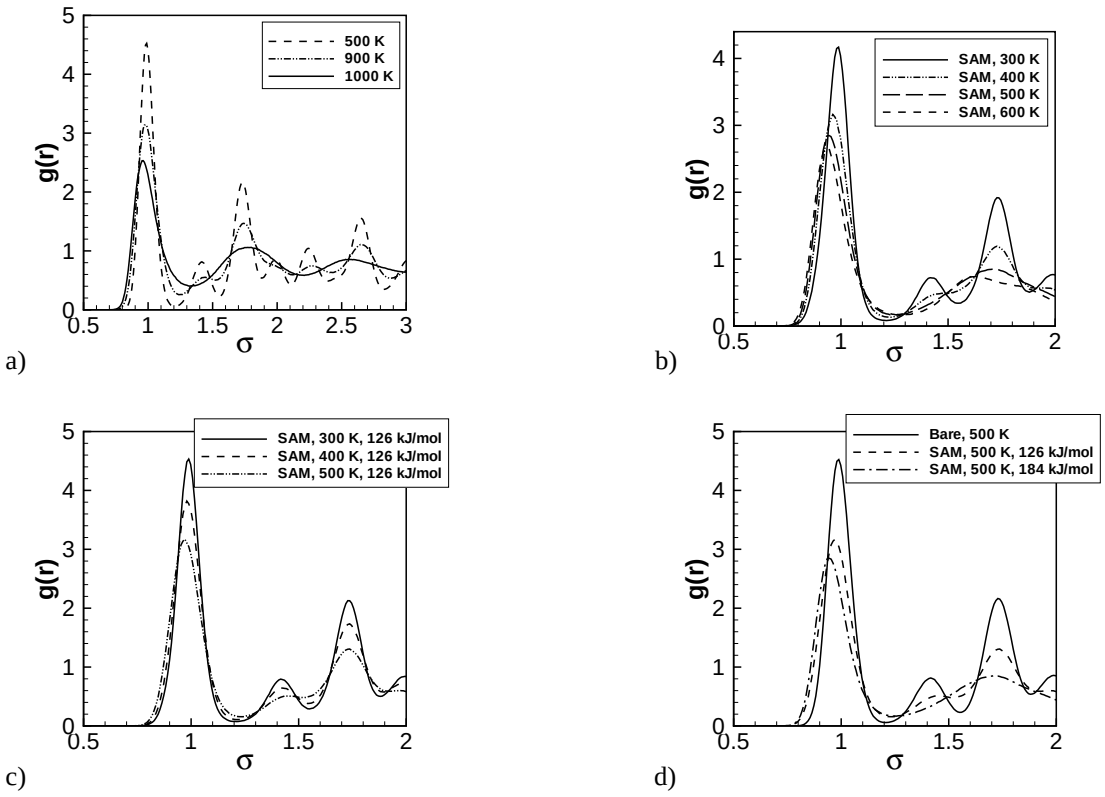

Figure 2. a) Pair correlation function for bare 50Å gold nanoparticle. Note the change in shape and the location of peaks between 900 K and 1000 K indicating a phase change from solid to liquid. **b)** Pair correlation function results for the gold atoms in a 50Å gold nanoparticle coated with an alkanethiolate SAM at various temperatures with a sulfur binding energy of 184 kJ/mol. **c)** The pair correlation function results for the SAM coated gold nanoparticle with the lower sulfur binding energy of 126 kJ/mol. **d)** a comparison of the pair correlation results at 500 K for the bare nanoparticle and high (184 kJ/mol) and low (126 kJ/mol) alkanethiol binding energies.

The results in Figure 2a indicate that a phase transition occurs in the nanoparticle from a crystalline solid at 900 K to a liquid at 1000 K, and as expected, this temperature range is below that of the bulk melting temperature of 1340 K.[44]

For a spherical nanoparticle the melting temperature can be crudely predicted from experimental data using Eq. 2, where ρ_S and ρ_L are the specific mass of the solid and liquid phases, respectively. γ_S and γ_L are the surface energies of the solid and liquid phases, respectively, D_p is the particle diameter, L is the heat of fusion, and T_∞ and $T(D_p)$ are the bulk and size dependent melting temperatures, respectively. Using published data for gold the predicted melting temperature of a 50Å diameter gold nanoparticle is about 995 K. This result is within the range of our MD simulation prediction for the melting temperature.

$$\frac{T(D_p)-T_\infty}{T_\infty}=\frac{4}{\rho_S L D_p}\left[\gamma_S-\gamma_L\left(\rho_S/\rho_L\right)^{2/3}\right] \tag{2}$$

Next we compare the pair correlation function results for the uncoated gold nanoparticle to the results for an alkanethiolate coated gold nanoparticle. The coating considered is a full coating, meaning one chain per 15.4Å^2 of surface area on the gold nanoparticle[45], and is about 30% denser than the packing density on a flat surface (21.4Å^2). The pair correlation function results for the alkenthiolate SAM-coated gold nanoparticle show a nanoparticle with a crystalline structure for temperatures below 400 K, and an amorphous structure above 600 K, see Figure 2b. The pair correlation function is computed for the gold atoms only in Figure 2b. By only considering the gold atoms in computing the pair correlation results, the structure of the nanoparticle is analyzed separately from the SAM. At 500 K, the structure of the gold nanoparticle has changed to a less ordered structure, similar to that observed during the melting of the uncoated gold nanoparticle. This change in the pair correlation function indicates that a phase change occurs in the gold nanoparticle between 400 K and 500 K. Hence the melting temperature of the gold nanoparticle is lowered by about 500 K by mixing with the alkanethiolate chains.

In the next set of simulations we considered the lower gold-sulfur binding energy of 126 kJ/mol. In these simulations the chain-chain interactions use the same interaction potentials discussed earlier. In Figure 2c the pair correlation results for the fully coated gold nanoparticle are plotted for temperatures of 300K, 400K, and 500K. Notice that at 500K the nanoparticle is still highly structured. This indicates that the nanoparticle does not undergo a phase change at 500K as is observed in the high binding energy results. In Figure 2d the pair correlation results for the gold nanoparticle at 500K is compared for the uncoated, and coated nanoparticles with high and low binding energy. In this figure the affect of the high binding energy is clearly evident. The lower degree of crystallinity with the higher binding energy indicates a more liquid-like structure at 500K.

3.2. Diffusion

From the results of the previous section it is apparent that the alkanethiolate SAM coating has an appreciable affect on the properties of the gold nanoparticle. In order to gain a better understanding of the SAM, and how it interacts with the gold nanoparticle we have computed the diffusion coefficient for the SAM and the gold atoms. The alkanethiolate chain is primarily bound to the gold nanoparticle through the sulfur-gold interactions at the head of the chain. The diffusion coefficient of the sulfur atoms is of particular interest because it will provide insight into the mobility of the alkanethiol chains in relation to the surface gold atoms. The diffusion coefficient of the alkanethiolate chain is calculated in the MD simulations by computing the mean squared displacement of the sulfur head group. The diffusion coefficient, D, is then evaluated using Eq. 3.

$$\frac{\partial\left\langle r^2(t)\right\rangle}{\partial t} = 2dD \tag{3}$$

In Eq. 3, the number of dimensions available for atomic diffusion, d, is assumed to be 3, t is time, and $\left\langle r^2(t)\right\rangle$ is the mean squared displacement (MSD) of the atoms being tracked. For diffusion on a surface, d would typically be 2. However, for a nanoparticle, as opposed to a flat surface, the gold atoms near the nanoparticle surface are less strongly bound to the core atoms, and thus more mobile, allowing for the sulfur atoms to move in a third dimension normal to the nanoparticle surface. This movement normal to the nanoparticle surface has not previously been considered in the simulation of SAM coated gold nanoparticles, but is expected for the reasons discussed previously.

The diffusion coefficient of the sulfur head group has been computed for various system temperatures and presented in an Arrhenius plot in Figure 3. There are two linear regions with slopes of -285.9 and -3477.6, indicating two distinct phases of the alkanethiolate SAM in the temperature ranges of 100 K – 500 K and 500 K – 800 K, respectively.

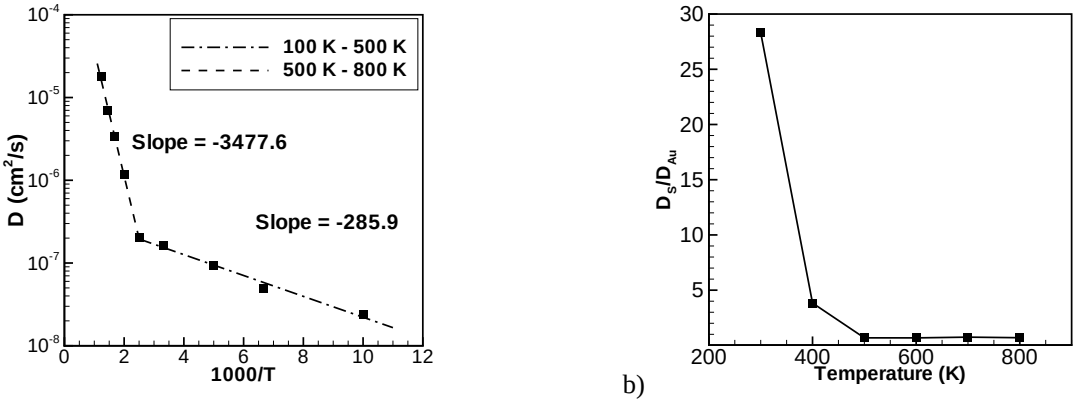

Figure 3. a) Arrhenius plot of diffusivity for sulfur atoms. The activation energy for SAM mobility is estimated by the slope of $\ln(D)$ vs. $1/T$ between 100 K and 800 K. **b)** Ratio of sulfur diffusivity to gold diffusivity in the alkanethiol coated gold nanoparticle material system.

The activation energy for the low and high temperature regions is 2.4 kJ/mol and 29.0 kJ/mol respectively. This is the expected behavior for heterodiffusion, where one type of atom diffuses on another.[46,47] In the low temperature regime the observed activation energy corresponds to the alkanethiol chains hopping between adsorption sites, which is observed as diffusion. For flat gold surfaces, particularly the Au(111) surface, the adsorption binding energy surface has been computed using atomistic simulations.[17,48] These atomistic computations have determined that the difference between the minimum binding energy (face-centered cubic) site, and the maximum binding energy (atop) site is

between 25.1 kJ/mol and 16.9 kJ/mol. The diffusion barrier is the energy required for an adsorbate atom to move to the next adsorption site. In Zhang et al. the authors have calculated the binding energy at a bridge site that would provide a possible diffusion path between adsorption sites with a diffusion barrier of 12.2 kJ/mol. Each of these published results are for flat surfaces, and report a somewhat higher activation energy than the computed activation energy from the MD simulations for the low temperature regime. One possible explanation for the discrepancy in the calculated value is that for a curved nanoparticle surface their may be lower energy and irregular diffusion paths available for the alkanethiolate chains to diffuse along. More likely however is that all the observed activation energies are small and in part at least differences may by associated with the accuracy of the interatomic potential. Nevertheless, is does indicate a significant difference between a low temperature diffusion process, and that occurring at higher temperature.

Typically, as the temperature rises the dominant mechanism for diffusion shifts from adatoms to vacancies. However, what is occurring here is that the diffusion of the alkanethiolate chain is dominated by dissolution into the gold nanoparticle, resulting in a more highly activated process. In both instances the activation energy required for diffusion is increased, but in the former process the change in activation energy is observed to be a factor of two or more. In this case the change is about one order of magnitude. The driving force for dissolution will be discussed in the next section. We notice however, in Figure 3b, that the diffusivity of the gold atoms is more than an order of magnitude lower than the sulfur head group atoms at low temperatures, below 500 K. This difference suggests that the alkanethiol chains are moving freely over the gold nanoparticle surface, but at around 500K this is no longer the case, and the diffusivity of the sulfur atoms closely tracks that of the gold nanoparticle atoms. Above 500K the diffusivity of the gold and sulfur atoms is similar, supporting the observation that mixing of the two materials has occurred.

3.3. Radial Pressure Distribution

The radial pressure distribution is used in this work to quantify the affect of the adsorbed alkanethiolate SAM on the gold nanoparticle. In very small droplets the internal pressure can be much larger than the surrounding environment. One method of evaluating the radial pressure distribution is to use the normal component of the Irving-Kirkwood (IK) pressure tensor.[49] The IK pressure tensor comprises two terms, corresponding to a kinetic $P_K(r,T)$ and a configurational $P_U(r,u)$ contribution as shown in Eq. 4.

$$P_N(r) = P_K(r,T) + P_U(r,u) \tag{4}$$

The kinetic pressure term is a function of temperature and the computed radial density distribution. The configurational term is computed from the interactions, u, between pairs of particles. For each shell of radius r, the forces between particles whose line of interaction intersects the shell is considered when computing the normal pressure component. The normal pressure at the surface of a nanoparticle or droplet is typically positive, indicating a compressive surface tension. Near the melting temperature of the gold nanoparticle the surface tension is computed to be nearly the published data of 742 *mN/m.*

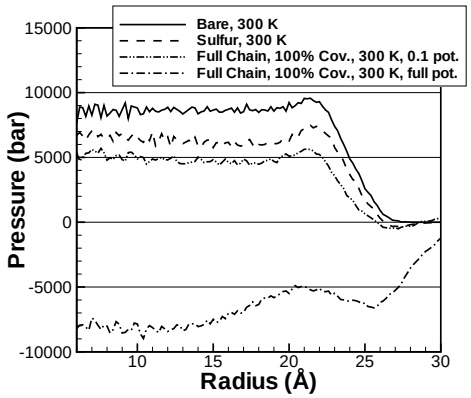

Figure 4. Radial pressure distribution for 50Å gold nanoparticle with alkanethiolate SAMs with differing interaction coefficients.

From past efforts it is expected that a surface coating will modify the nanoparticle internal pressure, through the surface tension, of the gold nanoparticle. This possibility is considered here by comparing the radial pressure distribution for gold nanoparticles with varying degrees of surface coatings. The systems considered include a bare gold nanoparticle, a gold nanoparticle with only sulfur atoms adsorbed onto the surface, and finally a gold nanoparticle with

alkanethiolate chains adsorbed on the surface, but with varying interaction potentials. For bare and coated gold nanoparticles with weak SAM chain-chain interactions the internal pressure is positive, meaning a positive surface tension. This result is expected, and the trend is also reasonably expected from past research involving hydrogen passivated silicon nanoparticles. As observed in Figure 4, the pressure trends lower, and becomes negative on the interior of the fully coated nanoparticle as the chain-chain and chain-gold interaction potential parameter values are increased to the published values, indicated by "Full Chain, 100% Cov., 300 K, full pot.".

As a first interpretation of this negative pressure result, one could consider the volume integral of the internal pressure distribution. Since the volume integral of the pressure distribution is negative, it indicates a mechanically unstable system, or a nanoparticle under tension. As seen in Figure 4, the negative pressure is observed in the interior of the nanoparticle, and only when full chain-chain and chain-gold interactions are considered. This negative pressure result indicates that the gold nanoparticle is experiencing a tensile stress and will change its configuration over time or with increases in temperature in order to accommodate the positive stress or negative pressure. The chain-chain interactions apparently have a strong influence on the surface tension, and therefore the internal pressure of the nanoparticle. The strength of the interaction potential that will flip the internal pressure from positive and mechanically stable, to negative and mechanically unstable is still under investigation but is between 10% and 100% of the published potentials used for the alkanethiolate SAM interaction potential. Other factors that may affect the surface tension are the surface area per adsorbed alkanethiol chain, and temperature.

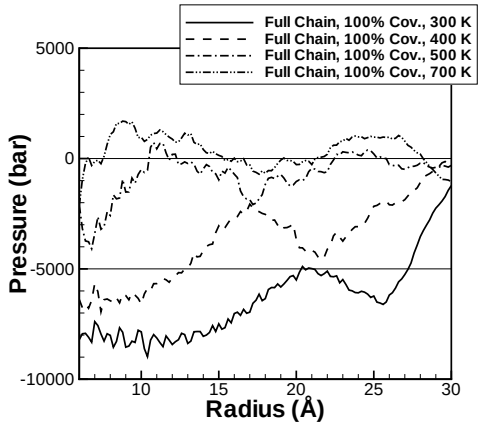

Figure 5. Radial pressure distribution for fully coated gold nanoparticle for range of temperatures with high binding energy (184.1 kJ/mol).

In Figure 5 the radial pressure profile is plotted for a fully coated gold nanoparticle with a sulfur gold binding energy of 184.1 kJ/mol. Notice that as the temperature increases the pressure that is primarily negative at 300 K becomes positive at 700 K. As the system is held at a temperature above the melting temperature of the solution the pressure continues to increase and will most likely equilibrate to an average pressure above 0.

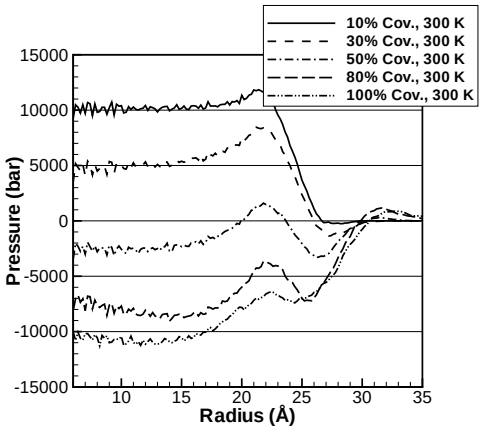

Figure 6. Radial pressure distribution for alkanethiol coated 50Å gold nanoparticle with 126 kJ/mol sulfur-gold binding energy.

A negative surface tension resulting in a tensile stress inside the nanoparticle is not stable for a liquid nanoparticle, and will result in deformation. In a solid nanoparticle the tensile stress will exist for a time before creep[50] or an increase in temperature will lower the yield strength allowing the nanoparticle to yield and flow. For these reasons the solid gold nanoparticle with an alkanethiolate coating is meta-stable at low temperatures, but will stabilize at higher temperatures by changing shape. In this particular case, we observed as discussed in the section on diffusion that the alkylthiol chains dissolve into the particle. This result has not been previously observed in computer simulations because the gold nanoparticle was assumed to maintain its shape, with the interaction of the alkanethiolate SAM constrained to the surface. Using the lower, 126 kJ/mol, binding energy we initially observe desorbtion of alkanethiolate chains from the nanoparticle surface as the temperature is increased, until the temperature is above 600K at which time the remaining alkanethiolate chains dissolve into the nanoparticle.

Notice in Figure 6 that the internal pressure of the fully coated nanoparticle with the 126 kJ/mol sulfur binding energy is very similar to the internal pressure of the fully coated gold nanoparticle in Figure 4, where the binding energy of the sulfur-gold bond is 184 kJ/mol. Recall that only the sulfur-gold binding energy has been changed in Figure 6, whereas in Figure 4 the "0.1 pot." curve represents data collected from simulations where the sulfur-gold and the chain-chain interactions have both been modified. By comparing these results we can conclude that the chain-chain interactions have a greater affect on internal pressure than the sulfur-gold binding energy. This is an important result because although the sulfur-gold binding energy has some affect on the structure of the gold nanoparticle and diffusivity, it is not the primary factor in determining stability of the nanoparticle. Additionally, the affect of chain length on the radial pressure distribution is also considered. After computing the radial pressure distribution for alkanethiol chain lengths of 3 and 18 carbon atoms, we have found that the shorter chains result in an internal pressure about 5000 bar higher than the previously considered 9 carbon atom chains. Alternatively, the longer chains don't appear to have a greater affect on the internal pressure of the nanoparticle than the 9 carbon atom chains studied here. This leads to the conclusion that for the number of monomers considered, a longer chain has little affect on the stability of the nanoparticle, whereas a shorter chain will lower the total chain-chain interaction sufficiently to affect the nanoparticle stability.

4. Phase Behavior and SAM Solubility

The computed potential energy (PE) of the alkanethiolate SAM coated gold nanoparticle system is used to determine the critical temperature at which mixing and phase change will occur. The computed slope of the PE versus temperature curve from the MD simulation results are used to determine the heat capacity of the system.

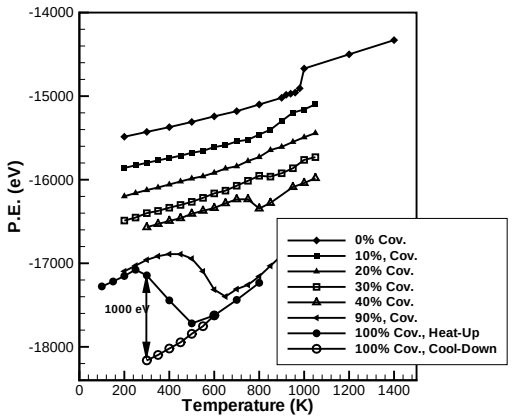

Figure 7. Potential energy versus temperature for the alkanethiolate SAM coated gold nanoparticle with various amount of surface coverage and the 184 kJ/mol sulfur binding energy.

In Figure 7, the system PE is plotted versus temperature for a 50Å gold nanoparticle coated with increasing densities of the alkanethiolate SAM. For the bare nanoparticle there is a discontinuity around 980 K, which corresponds to a phase change. The SAM coated nanoparticle demonstrates a very different behavior. Initially, for small numbers of adsorbed alkanethiolate chains, the melting temperature of the gold nanoparticle decreases, and does not occur at a unique temperature but rather over a range of temperatures. This behavior is expected for a mixture of two materials. The appearance of the SAM on the particle surface decreases the surface tension and internal pressure. As the coverage percentage is increased further, another behavior is observed. At higher surface coverages, above 70%, the PE of the system begins to decrease as the temperature is increased, and then after a small temperature range the PE resumes its linear increase. This behavior is explained by the mixing that occurs between the alkanethiolate chains and the gold

atoms. The mixing of the SAM chains with the gold atoms is possible because of the lower binding energy of surface Au atoms. The lower binding energy of the surface atoms allows these atoms to become mobile at a lower temperature than the interior gold atoms. The surface atoms begin to mix with the alkanethiol chains, and as the chains penetrate deeper into the nanoparticle they are able to interact with an ever increasing number of gold atoms. Once complete mixing has occurred, the PE resumes increasing monotonically.

As we found with the internal pressure in Figure 4, the structure of the SAM coated gold nanoparticle is metastable. The increase of both the surface coverage, and the temperature aids this particle in transforming into a mixed structure, Figure 8. This result has not been previously predicted, as it was previously assumed that the SAM chains would desorb at these temperatures, as occurs on flat surfaces. If the SAM was to desorb, it is expected that the structure of the underlying gold nanoparticle would not be affected. This is reflected in the pair correlation data discussed earlier that shows that the gold nanoparticle with SAM coating is crystalline at a higher temperature with the lower 126 kJ/mol sulfur binding energy than with the 184 kJ/mol binding energy.

a) **b)**

Figure 8. Cross section of 100% coated gold nanoparticle at 300K (a) and 600K (b), showing the dissolution of the alkanethiol chains at high temperatures. In these images the blue spheres represent gold atoms, light blue are sulfur, yellow are CH_2 and red spheres represent CH_3.

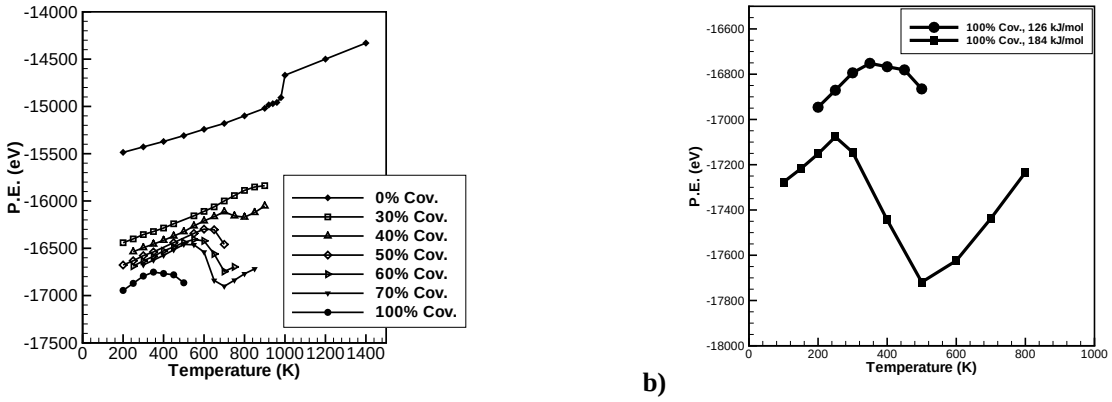

a) **b)**

Figure 9. a) Potential energy versus temperature for the alkanethiolate SAM coated gold nanoparticle with various amount of surface coverage and 126 kJ/mol binding energy. b) Comparison of potential energy versus temperature for fully coated nanoparticle with 184 kJ/mol and 126 kJ/mol binding energy.

In Figure 9a, the PE for the 126 kJ/mol sulfur binding energy simulation is plotted. During these simulations, as opposed to the 184 kJ/mol binding energy simulations, we observed some desorbtion of alkanethiol chains from the gold surface. This desorbtion process is irreversible because of the low density of desorbed chains in the simulation volume, a realistic assumption for coated nanoparticles in a vacuum or near vacuum. In Figure 9b it is interesting to note that the temperature at which the decrease in PE occurs for the 126 kJ/mol sulfur binding energy is higher than the 184 kJ/mol binding energy simulations. This result confirms the observation that when considered with a lower sulfur binding energy that the alkanethiol chains have a lower propensity to dissolve into the gold nanoparticle and a higher probability of desorbing from the gold surface.

The enthalpy of solution, H_{sol}, can be computed from the PE data. The enthalpy of solution is computed as the difference in system internal energy, between the undissolved SAM chain system prior to heating and the internal energy of the same system after cooling down to the same temperature. The PE of the system decreases as a result of the mixing that occurs in the fully coated gold nanoparticle model during an increase in temperature from 300 K to 600 K.

This mixing may potentially occur completely at 300 K if it were possible to simulate long times (greater than 10 ns) in the MD simulations performed here. On the other hand, it is also possible that the activation energy for this transition to occur may be too high to complete the transition at 300 K. The measured change in system PE is 1000 eV, which is the enthalpy of solution.[51] Denoting this result per unit mass of the fully coated gold nanoparticle results in an enthalpy of solution of 100 kJ/kg. These results show that the SAM has a measurable affect on not only the nanoparticle surface but the entire system.

Conclusions

The alkanthiolate SAM-coated gold nanoparticle has been shown to be mechanically and chemically metastable. The SAM that is adsorbed onto the surface begins to mix with the surface gold atoms at low temperatures because of the weaker gold-gold bonding of the surface atoms to the interior gold atoms. This process is more pronounced as the density of the SAM is increased and as the gold-sulfur binding energy is increased. This is demonstrated by the corrugation numbers computed previously. For full surface coverage, the SAM chains will begin to diffuse into the gold core as the temperature rises from 300 K to 500 K. This mixing process lowers the PE of the system. The diffusion activation energy of the sulfur atoms is measured to be low in this temperature range. Once the temperature has increased to around 600 K, the alkanethiolate chains are completely mixed with the gold atoms, and the activation energy for diffusion greatly increases. The PE and diffusivity results concur with this observation that a phase change in the SAM-coated gold nanoparticle system occurs around 500 K. We have therefore concluded that the melting temperature of the gold is lowered by the adsorption of alkanethiolate SAMs on the nanoparticle surface and creates a metastable system for fully covered nanoparticles of diameters around 50Å. The measured decrease in melting temperature of the nanoparticle is more pronounced as more SAM chains are adsorbed onto the nanoparticle surface.

We have also compared each of the computed results for the low, 126 kJ/mol, gold-sulfur binding energy reported in the literature to the results from the high, 184 kJ/mol binding energy. These comparisons show that the gold-sulfur binding energy does not have a large affect on the meta-stability of the nanoparticle. From these results we are able to conclude that the primary factor in determining if a nanoparticle will become meta-stable is the strength of the chain-chain interactions. Since experiments concur that desorbtion occurs in the 300K to 550K temperature range we have concluded that the 126 kJ/mol binding energy is most likely a better estimate of the true binding energy than the 184 kJ/mol value. Independent of the binding energy is the tilt angle, which is found to be greater for the nanoparticle geometry than for a flat surface.

Acknowledgements

The authors would like to acknowledge the support received by the U.S. Army Major Shared Resource Center (MSRC) at the Aberdeen Proving Ground, MD. Additional support was given by the National Institute for Standards Technology (NIST).

References

1. Manna, A.; Imae, T.; Aoi, K.; Okazaki, M. *Mol. Sim.* **2003**, 29(10–11), 661–665.

2. Hong, R.; Han, G.; Fernández, J. M.; Kim, B.–J.; Forbes, N. S.; Rotello, V. M. *J. Am. Chem. Soc.* **2006**, 128, 1078–1079.

3. Magnusson, M. H.; Duppert, K.; Malm, J.–O.; Bovin, J.–O.; Samuelson, L. *NanoStructured Materials* **1999**, 12, 45–48.

4. Chiang, C.–L. *J. of Colloid and Interface Science* **2000**, 230, 60–66.

5. Kim, J.–U.; Cha, S.–H.; Shin, K.; Jho, J. Y.; Lee, J.–C. *J. Am. Chem. Soc. Communications* **2005**, 127, 9962–9963.

6. Landman, U.; Luedtke, W. D. *Faraday Discussions* **2004**, 125,1–22.

7. Schreiber, F. *Progress in Surface Science* **2000**, 65,151–256.

8. Greer, J. R.; Nix, W. D. *Applied Physics A* **2005**, 80,1625–1629.

9. Cleveland, C. L.; Landman, U.; Schaaff, T. G.; Shafigullin, M. R.; Stephens, P. W.; Whetten, R. L. *Phys. Rev. Lett.* **1997**, 79(10), 1873–1876.

10. Baskes, M. I. *Phys. Rev. B* **1997**, 46(5), 2727–2742.

11. Daw, M. S.; Baskes, M. I. *Phys. Rev. B* **1984**, 29(12), 6443–6453.

12. Lewis, L. J.; Jensen, P.; Barrat, J. –L. *Phys. Rev. B* **1997**, 56(4), 2248–2257.

13. Shevade, A. V.; Zhou, J.; Zin, M. T.; Jiang, S. *Langmuir* **2001**, 17, 7566–7572.

14. Nuzzo, R. G.; Zegarski, B. R.; Dubois, L. H. *J. Am. Chem. Soc.* **1987**, 109, 733–740.

15. Strong, L.; Whitesides, G. M. *Langmuir* **1988**, 4, 546–558.

16. Rosenbaum, A. W.; Freedman, M. A.; Darling, S. B.; Popova, I.; Sibener, S. J. *J. Chem. Phys.* **2004**, 120(8), 3880–3886.

17. Zhang, L.; Goddard III, W. A.; Jiang, S. *Computers in Chem. Eng.* **2002**, 22(10), 1381–1385.
18. Luedtke, W. D.; Landman, U. *J. Phys. Chem.* **1996**, 100(32), 13323–13329.
19. Jiang, S. *Mol. Phys.* **2002**, 100(14), 2261–2275.
20. Bhatia, R.; Garrison, B. J. *Langmuir* **1997**, 13, 765–769.
21. Masens, C.; Ford, M. J.; Cortie, M. B. *Surf. Sci.* **2005**, 580, 19–29.
22. Hawa, T.; Zachariah, M. R. *Phys. Rev. B* **2004**, 69, 035417.
23. Hawa, T.; Zachariah, M. R. *Phys. Rev. B* **2005**, 71, 165434.
24. Hawa, T.; Zachariah, M. R. *J. Chem. Phys.* **2004**, 121(18), 9043–9049.
25. Grönbeck, H.; Curioni, A.; Andreoni, W. *J. Am. Chem. Soc.* **2000**, 122, 3839–3842.
26. Plimpton, .S. J. *J. Comp. Phys.* **1995**, 117, 1–19.
27. Foiles, S. M.; Baskes, M. I.; Daw, M. S. *Phys. Rev. B* **1986**, 33(12), 7983–7991.
28. Mei, J.; Davenport, J.W.; Fernando, G.W. *Phys. Rev. B* **1991**, 43(6), 4653–4658.
29. Lee, B.; Cho, K. *Surf. Sci.* **2006**, 600, 1982–1990.
30. Haftel, M. I. *Phys. Rev. B* **1993**, 48(4), 2611–2622.
31. Jorgensen, W. L.; Madura, J. D.; Swenson, C. J. *J. Am. Chem. Soc.* **1984**, 106, 6638–6646.
32. Fukunaga, H.; Takimoto, J. i.; Doi, M. *J. Chem. Phys.* **2002**, 116(18), 8183–8190.
33. Tries, V.; Paul, W.; Baschnagel, J.; Binder, K. *J. Chem. Phys.* **1997**, 106(2), 738–748.
34. Maiti, P. K.; Lansac, Y.; Glaser, M. A.; Clark, N. A. *Langmuir* **2002**, 18, 1908–1918.
35. Rai, B.; Sathish, P.; Malhotra, C. P.; Pradip; Ayappa, K. G. *Langmuir* **2004**, 20, 3138–3144.
36. Mahaffy, R.; Bhatia, R.; Garrison, B. J. *J. Phys. Chem. B* **1997**, 101, 771–773.
37. Beardmore, K. M.; Kress, J. D.; Gronbech-Jensen, N.; Bishop, A. R. *Chem. Phys. Lett.* **1998**, 286, 40–45.
38. Hautman, J.; Klein, M. L. *J. Chem. Phys.* **1989**, 91(8), 4944–5001.
39. Liu, K. S. S.; Yong, C. W.; Garrison, B. J.; Vickerman, J. C. *J. Phys. Chem. B* **1999**, 103, 3195–3205.
40. Lavrich, D. J.; Wetterer, S. M.; Bernasek, S. L.; Scoles, G. *J. Phys. Chem. B* **1998**, 102, 3456–3465.
41. Jang, S. S.; Jang, Y. H.; Kim, Y.-H.; Goddard III, W. A.; Flood, A. H.; Laursen, B. W.; Tseng, H.-R.; Stoddart, J. F.; Jeppesen, J. O.; Choi, J. W.; Steuerman, D. W.; Delonno, E.; Heath, J. R. *J. Am. Chem. Soc.* **2005**, 127, 1563–1575.
42. Henz, B. J.; Hawa, T.; and Zachariah, M. R. *Langmuir* **2008**, 24(3), 773–783.
43. Allen, M. P.; Tildesley, D. J. *Computer Simulation of Liquids*. Oxford University Press Inc., New York, NY, 1987.
44. Lewis, L. J.; Jensen, P.; Barrat, J. –L. *Phys. Rev. B* **1997**, 56(4), 2248–2257.
45. Badia, A.; Cuccia, L.; Demers, L.; Morin, F.; Lennox, R. B. *J. Am. Chem. Soc.* **1997**, 119, 2682–2692.
46. Dalton, A. S.; Seebauer, E. G. *Surf. Sci.* **2007**, 601, 728–734.
47. Suni, I. I. *Surf. Sci.* **1995**, 309, L179–L183.
48. Sellers, H.; Ulman, A.; Shnidman, Y.; Eilers, J. E. *J. Am. Chem. Soc.* **1993**, 115, 530–542.
49. Thompson, S. M.; Gubbins, K. E.; Walton, J. P. R. B.; Chantry, R. A. R.; Rowlinson, J. S. *J. Chem. Phys.* **1984**, 81(1), 530–542.
50. Dieter, G. E. *Mechanical Metallurgy*. McGraw-Hillm Inc., New York, NY, 1986.
51. Winn, J. S. *Physical Chemistry*. Addison Wesley, Boston, MA, 1995.